

NEAR-INFRARED AND OPTICAL MORPHOLOGY OF THE DUSTY GALAXY NGC 972

Y. D. MAYYA,¹ SWARA RAVINDRANATH,² AND L. CARRASCO^{1,3}

Received 1998 June 12; revised 1998 July 8

ABSTRACT

Near-infrared (NIR) and optical surface photometric analyses of the dusty galaxy NGC 972 are presented. The photometric profiles in the *BVRJHK* bands can be fitted with a combination of Gaussian and exponential profiles, corresponding to a starburst nucleus and a stellar disk, respectively. The exponential scale length in the *B* band is 2.8 times larger than in the *K* band, which implies a central *B*-band optical depth as high as 11. A bulge is absent even in the NIR bands, and hence the galaxy must be of a morphological type later than the usually adopted Sb type. Relatively low rotational velocity and high gas content also favor a later type, probably Sd, for the galaxy. Only one arm can be traced in the distribution of old stars; the second arm, however, can be traced in the distribution of dust and H II regions. Data suggest a short NIR bar, which ends inside the nuclear ring. The slowly rising nature of the rotation curve rules out a resonance origin of the nuclear ring. The ring is most likely not in the plane of the galaxy, given its circular appearance, in spite of the moderately high inclination of the galaxy. The off-planar nature of the star-forming ring, the unusually high fraction (30%) of the total mass in molecular form, the presence of a nuclear starburst, and the asymmetry of spiral arms are probably the result of a merger with a gas-rich companion galaxy.

Key word: dust, extinction — galaxies: individual (NGC 972) — galaxies: structure

1. INTRODUCTION

NGC 972 is a nearby dusty galaxy whose morphological type is yet to be established. It is classified as Sb in the Hubble Atlas of Galaxies (Sandage 1961), the Third Reference Catalogue of Bright Galaxies (de Vaucouleurs et al. 1991, hereafter RC3), and the Revised Shapley-Ames Catalog (Sandage & Tammann 1981). However, Krienke & Hodge (1974) found the galaxy to share many properties with I0-type galaxies, and accordingly the galaxy was given an I0 classification in the Second Reference Catalogue of Bright Galaxies (de Vaucouleurs, de Vaucouleurs, & Corwin 1976). Given the heterogeneity of the I0-class galaxies, the presence of a well-established trailing dusty arm (Burbidge, Burbidge, & Prendergast 1965) in this galaxy was taken as strong support in favor of the Sb classification. The presence of a star-forming nuclear ring in this galaxy, if assumed to be a resonance ring, also seems to support the Sb classification of the galaxy (Ravindranath & Prabhu 1998, hereafter RP98).

The optical appearance of NGC 972, which was the basis for its morphological classification hitherto, is dominated by the dust lanes. Interestingly, the presence of these dust lanes has played a major role in its classification both as Sb and I0—the dusty trailing arm supporting its Sb classification, the chaotic appearance caused by dust placing it in the class of I0 galaxies. This highlights the limitation of the qualitative classification schemes based solely on the optical morphologies, especially for dust-rich galaxies such as NGC 972. Recent advances in observational techniques and theoretical modeling of galaxy dynamics allow us to use many more properties than just optical morphology to establish the true morphological type of galaxies. From the

observational side, near-infrared (NIR) imaging allows us to have a dust-free view of the underlying morphological components of galaxies. Such observations have already helped us discover new components such as nuclear spirals and bars in galaxies whose optical appearance did not suggest the existence of those components (Zaritsky, Rix, & Rieke 1993; Knapen et al. 1995). The variation of dynamical properties, such as the rotation speed, length of the bar, etc., along the Hubble sequence is now well understood. Early-type galaxies rotate faster than late-type galaxies (Zaritsky 1993). The bars of early-type galaxies are lengthy and uniform, whereas they are short and weak in late-type galaxies (Combes & Elmegreen 1993). Thus, galaxy classification can be done in an integrated way by making use of both the morphological and dynamical properties of galaxies. Such studies will also help in isolating the underlying physical quantities governing the Hubble sequence.

We carried out a quantitative morphological investigation of NGC 972 to check whether its Sb classification requires revision. We based our analysis on the newly obtained NIR images and made use of the existing optical images. In addition, we compiled the available information on the gas content, star formation indicators, and dynamics to infer its morphological type in an integrated way. We found that none of the quantitative indicators of the galaxy morphology favor its Sb classification, and the galaxy seems to be of type as late as Sd. Observations and the techniques followed in the reduction of the data are described in § 2. The main surface photometric results are presented in § 3, and the opacity of the disk of NGC 972 is discussed in § 4. Issues related to the morphological type and the dynamical history of the galaxy are discussed in § 5. Concluding remarks are given in § 6. A distance of 21.9 Mpc is adopted for the galaxy, based on the velocity from RC3, and a Hubble constant of $75 \text{ km s}^{-1} \text{ Mpc}^{-1}$. This results in an image scale of $105 \text{ pc arcsec}^{-1}$.

2. OBSERVATIONS AND DATA REDUCTION

Near-infrared observations were carried out using the CAMILA instrument (Cruz-Gonzalez et al. 1994) at the

¹ Instituto Nacional de Astrofísica, Óptica y Electrónica, Apdo. Postal 51 y 216, 72000 Puebla, Pue., Mexico; ydm@inaoep.mx, carrasco@inaoep.mx.

² Indian Institute of Astrophysics, Koramangala, Bangalore 34, India; cathy@iiap.ernet.in.

³ Also at Observatorio Astronómico de Nacional, Universidad Nacional Autónoma de México, Mexico.

2.1 m telescope of the Observatorio Astronómico Nacional at San Pedro Martir, Baja California. The CAMILA instrument uses a NICMOS 3 detector of 256×256 pixel format. The instrument was used in the imaging mode with the focal reducer configuration $f/4.5$ in all of our observations. This results in a spatial resolution of $0''.85 \text{ pixel}^{-1}$ and a total field of view of $3''.6 \times 3''.6$.

The imaging observations were carried out on the night of 1997 September 13 using the broadband filters J , H , and K' . Each observation consisted of a sequence of object and sky exposures, with the integration time of an individual exposure limited by the sky counts, which was kept well below the nonlinear regime of the detector. The net exposure times on the object were 12, 6, and 5 minutes for the J , H , and K' bands, respectively. Roughly equal amounts of time were spent on the sky fields. The recessional velocity of 1670 km s^{-1} for NGC 972 did not allow us to detect the $\text{Br}\gamma$ emission line with the available zero-redshift $\text{Br}\gamma$ filter. Photometric calibration to the standard JHK system was performed using the United Kingdom Infrared Telescope standard star FS 7 (Casali & Hawarden 1992). The sky conditions were photometric, and the sky magnitudes were roughly 15.9, 14.2, and 11.5 mag arcsec $^{-2}$ in the J , H , and K bands, respectively. The seeing FWHM was typically $2''.0$.

The image processing involved subtraction of the bias and sky frames, division by flat-field frames, registration of the images to a common coordinate system, and then stacking all of the images in a filter. Bias subtraction was carried out as part of the data acquisition. The sky frames in each filter were prepared by combining all of the sky frames using the median operation. Flat-field frames were taken during twilight period. A master flat-field frame for each filter was constructed by stacking several night-sky-subtracted twilight frames in corresponding filters. The flat-fielding operation involved dividing the sky-subtracted images of the object by normalized master flats. The resulting images were aligned to a common coordinate system using the common stars in the frames and then combined using the median operation. Only good images (as defined in the CAMILA manual—see Cruz-Gonzalez et al. 1994) were used for combining the images. Some of the images had a horizontal band at the joints of the individual chips forming the detector of the NICMOS 3 camera. We eliminated this feature by subtracting a 255×1 median smoothed image from the original images. The resulting combined images were aligned to the image from the Digitized Sky Survey through a geometrical mapping using the GEOTRAN and GEOMAP tasks available in the reduction software. The transformed star positions in the images agreed to within $0''.2$ as judged from the coordinates of common stars. Also, the images were assigned the equatorial coordinates using the image from the Digitized Sky Survey.

The routines under Image Reduction and Analysis Facility⁴ (IRAF) and Space Telescope Science Data Analysis System (STSDAS) were used in the reduction and analysis of all of the data. The optical images used in this study are from RP98.

3. MORPHOLOGICAL STRUCTURES

The most striking feature on the optical images of the galaxy is a dust lane running from southeast to northwest. The prominent spiral arm is on the northwest, partially broken by the dust lane. The second spiral arm in the symmetric position on the southeast is traced by the dust lane. The appearance of the dusty arm suggests that the southeast side is the near side of the galaxy. Burbidge et al. (1965) used this information along with the rotation curve to establish that the spiral arms are trailing in this galaxy. However, the stellar arm corresponding to the dusty arm cannot be traced on the optical images, which is probably due to the heavy obscuration.

The structure of the galaxy in the optical and NIR bands is shown as gray-scale maps in Figure 1. The K and B band images are shown in Figures 1*a* and 1*b*, whereas the $H-K$ and $J-K$ color maps are shown in Figures 1*c* and 1*d*, respectively. The galaxy has a smooth distribution of intensity in the NIR bands as compared to the optical bands. The dust lanes, which are prominent in the B -band image, are absent in the K -band image. The northwest spiral arm is easily traceable and continuous in all three NIR bands and coincides in position with that in the B band. However, the southeast stellar arm, which is expected to lie on the leading side of the dusty arm, cannot be traced even on NIR images. Instead, a linear spur can be traced on the NIR images on the inner side of the dust lane. The spur lies roughly parallel to the major axis of the galaxy and runs $\sim 5''$ south of the nucleus into the northwest side. The nucleus and the optically prominent H II region on the northwest can both be traced in the NIR bands, with the nucleus relatively brighter than the H II region. A bulge is not apparent on the NIR images. A short barlike extension along the north-south direction can be seen.

3.1. *Spiral Arms, Dust Lanes, and Star Formation*

Images in the K band are least affected by dust and hence are best suited to study the intrinsic components, such as the bulge, the disk, and the spiral arms of galaxies. On the other hand, the B -band images are heavily affected by the dust, and hence structural differences between B and K bands can be used to map the distribution of dust. Differences in stellar populations can also lead to structural differences between B and K bands (de Jong 1996). However, in dusty galaxies such as NGC 972, the major contribution to the observed structures on color images comes from the nonuniform distribution of dust rather than the stellar population gradients. Thus it can be assumed that the structures seen in the $B-K$ color image of NGC 972, to first order, represent the dust distribution. Contours of $B-K$ colors, drawn to illustrate the dust lanes, are shown superposed on the $H-K$ and $J-K$ color maps (Figs. 1*c* and 1*d*). The outer contour almost forms the boundaries of the structures seen in the NIR color maps, indicating that the dust absorption is nonnegligible even at NIR wavelengths in this galaxy.

Distribution of giant H II regions, as traced by $\text{H}\alpha$ emission, characterizes the regions of current star formation. $\text{H}\alpha$ emission in NGC 972 extends to 3.4 kpc (RP98) and is shown as a gray-scale map in Figure 2. K -band contours at levels selected to illustrate the disk shape, spiral arms, and the nuclear regions are superposed (thin double lines denoted by 1, 2, and 3, respectively) on the $\text{H}\alpha$ map. The

⁴ IRAF is distributed by National Optical Astronomy Observatories, which are operated by the Association of Universities for Research in Astronomy, Inc., under cooperative agreement with the National Science Foundation.

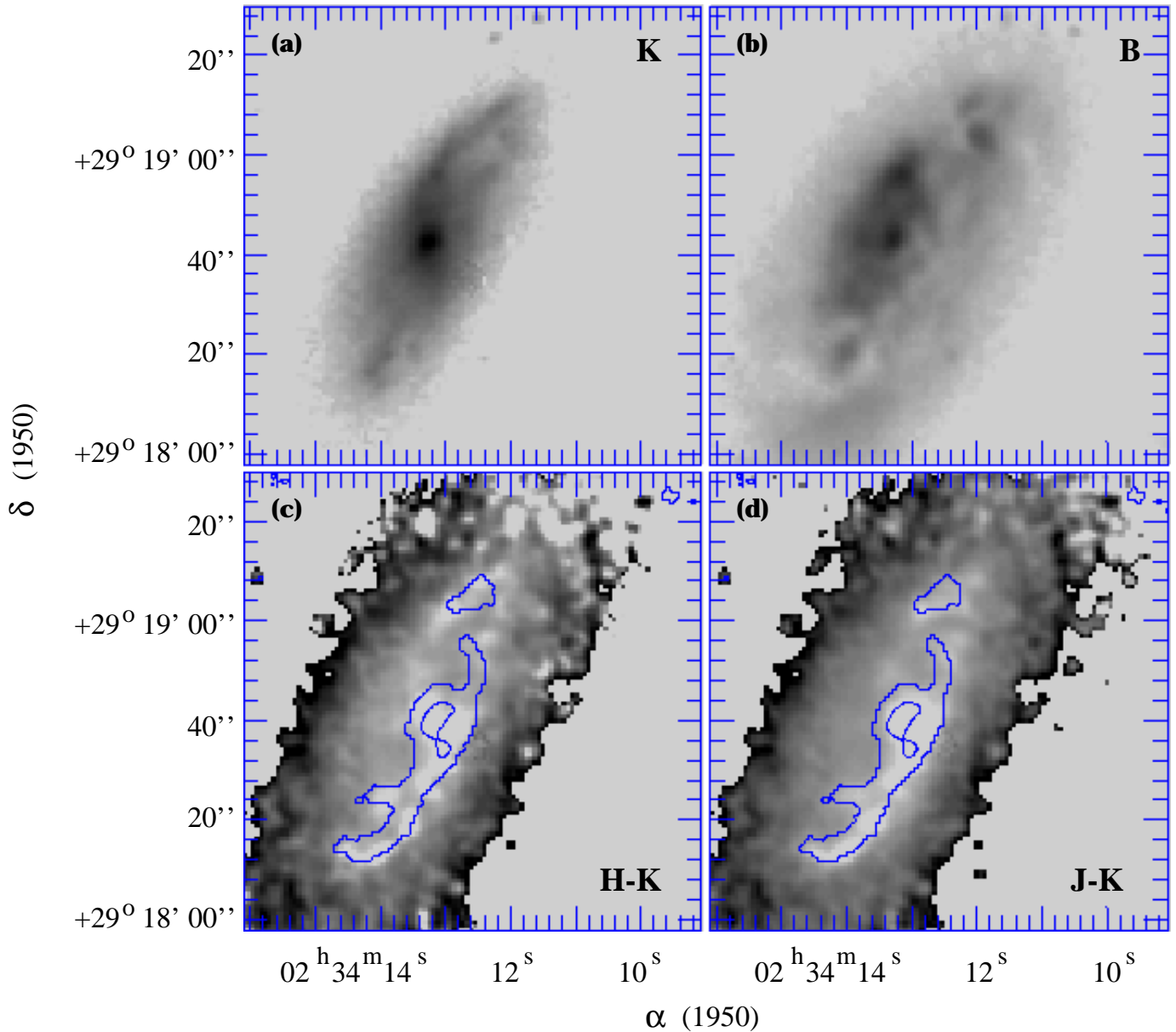


FIG. 1.—Gray-scale images of NGC 972 in (a) K band (b) B band (c) $H-K$ color and (d) $J-K$ color (brighter gray scales correspond to redder colors). Contours of $B-K$ color are superposed on the color maps and represent the position of the optically seen dust lane.

boundary of the principal structures seen on the $B-K$ color map are shown as contours (*thick lines*) in this figure. On the southeast side, these contours demarcate the leading edge of a dusty arm.

It can be seen that the star formation extends almost over the entire stellar disk as traced by the K -band isophote. Current star formation is active along the northwest spiral arm. The $H\ II$ region population can be traced along the southeast dusty arm as well. Significantly, these $H\ II$ regions lie on the convex side of the dusty arm, as is expected for a trailing density wave. $H\ II$ regions near the center of the galaxy are distributed along a partial nuclear ring of radius $6''$. Note that this ring is nearly circular in shape, whereas the outermost K -band isophote (contour numbered as 1) is highly elliptical. The central K -band contour (denoted as 3) is of oval shape and is elongated along the line connecting the beginning of the spiral arms. This suggests the presence

of a weak bar in the galaxy, which seems to end just inside the circumnuclear ring. There is a significant amount of star formation in the interarm regions of this galaxy.

3.2. Bar, Bulge, Nucleus, and Disk

Azimuthally averaged radial surface brightness profiles have been most widely used for a quantitative analysis of the morphological structures. K -band profiles are best suited for this purpose because of their ability to trace the old stellar population and also because they are least affected by the obscuring dust. However, the high background levels in the K band restrict the usable radius to within $1'$ of the center. On the other hand, J -band profiles are less affected by the sky background, and hence we carried out surface photometric analysis on the J profiles as well. Surface photometric analysis included fitting ellipses to the isophotes and the construction of the radial profiles

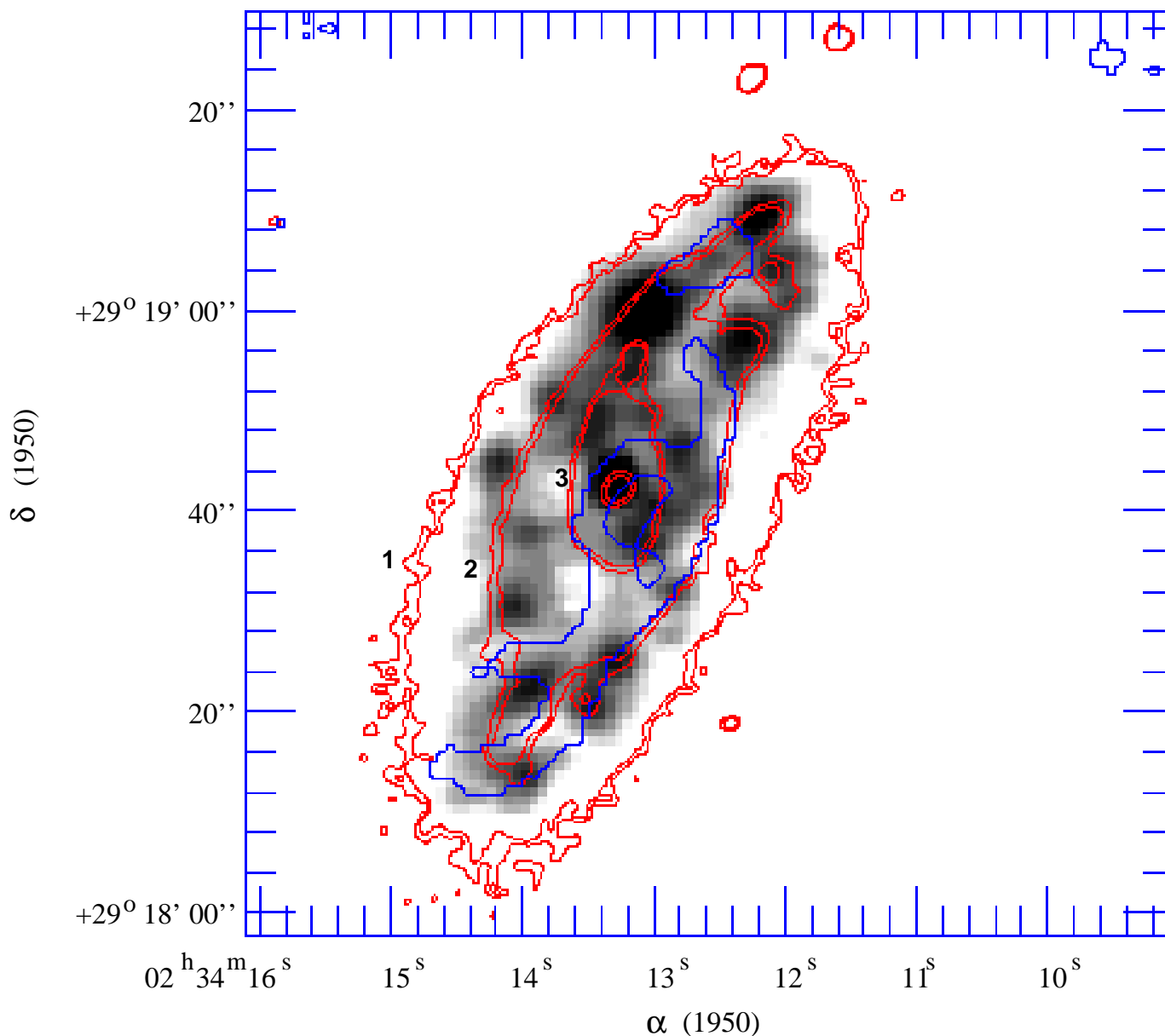


FIG. 2.—Isointensity contours in K band (*thin double line*) and $B-K$ color (*thick line*) are superposed on the gray-scale $H\alpha$ image of NGC 972. Four pairs of K contour levels are drawn and illustrate the outer structure, the spiral arm, the central weak bar (numbered 1, 2, and 3, respectively), and the nucleus. These contours correspond to surface brightness levels of 18.4, 16.9, 15.7, and 14.2 mag arcsec $^{-2}$, respectively. Two $B-K$ contours are drawn, corresponding to colors 4.75 (outer) and 5.50 mag. The outer $B-K$ contour traces the dust lane, running all the way from the southeast to the northwest spiral arm. Notice that the distribution of disk $H II$ regions follows the K -band spiral in the northwest and the dust lane on the southeast side. Another notable feature is the vastly different ellipticities of the $H\alpha$ nuclear ring (nearly circular) and the outer K -band isophote.

of isophote intensity, ellipticity (ϵ), and the position angle (P.A.) of the resulting ellipses. These were carried out using the ellipse-fitting routines under the STSDAS package.

The results of surface photometric analyses are plotted in Figure 3. The ellipticity and P.A. for the J and K bands are plotted in Figures 3a and 3b, respectively. Both of the plotted quantities attain a steady value (ellipticity = 0.60 and P.A. = 152 $^\circ$) at radii exceeding 35". The resulting P.A. is exactly equal to the optically measured value (RC3). However, the value of ellipticity suggests that the galaxy is marginally more elongated in the NIR compared to the optical value in RC3. Figures such as Figures 3a and 3b can be used to infer the presence of a bar, e.g., a strong bar would show up as a high eccentricity and a constant P.A. structure between the nucleus and the beginning of the

spiral arm. No such structure is obvious in Figures 3a and 3b, and hence a strong bar is absent in this galaxy. However, there is an indication for the presence of a small bar at P.A. = 170 $^\circ$, which ends inside a radius of 10". This weak bar can also be seen on the K -band image (Fig. 1a) as discussed earlier.

A quantitative estimate of the bulge-to-disk ratio of galaxies can be made by decomposing the radial intensity profiles into de Vaucouleurs $r^{1/4}$ and exponential profiles. We obtained azimuthally averaged radial intensity profiles by fixing the eccentricity and P.A. corresponding to their values at the outer radii. We fitted the radial intensity profiles with a composite profile containing a nucleus (Gaussian), a bulge ($r^{1/4}$), and an exponential disk. The profile shape is inconsistent with the presence of an $r^{1/4}$

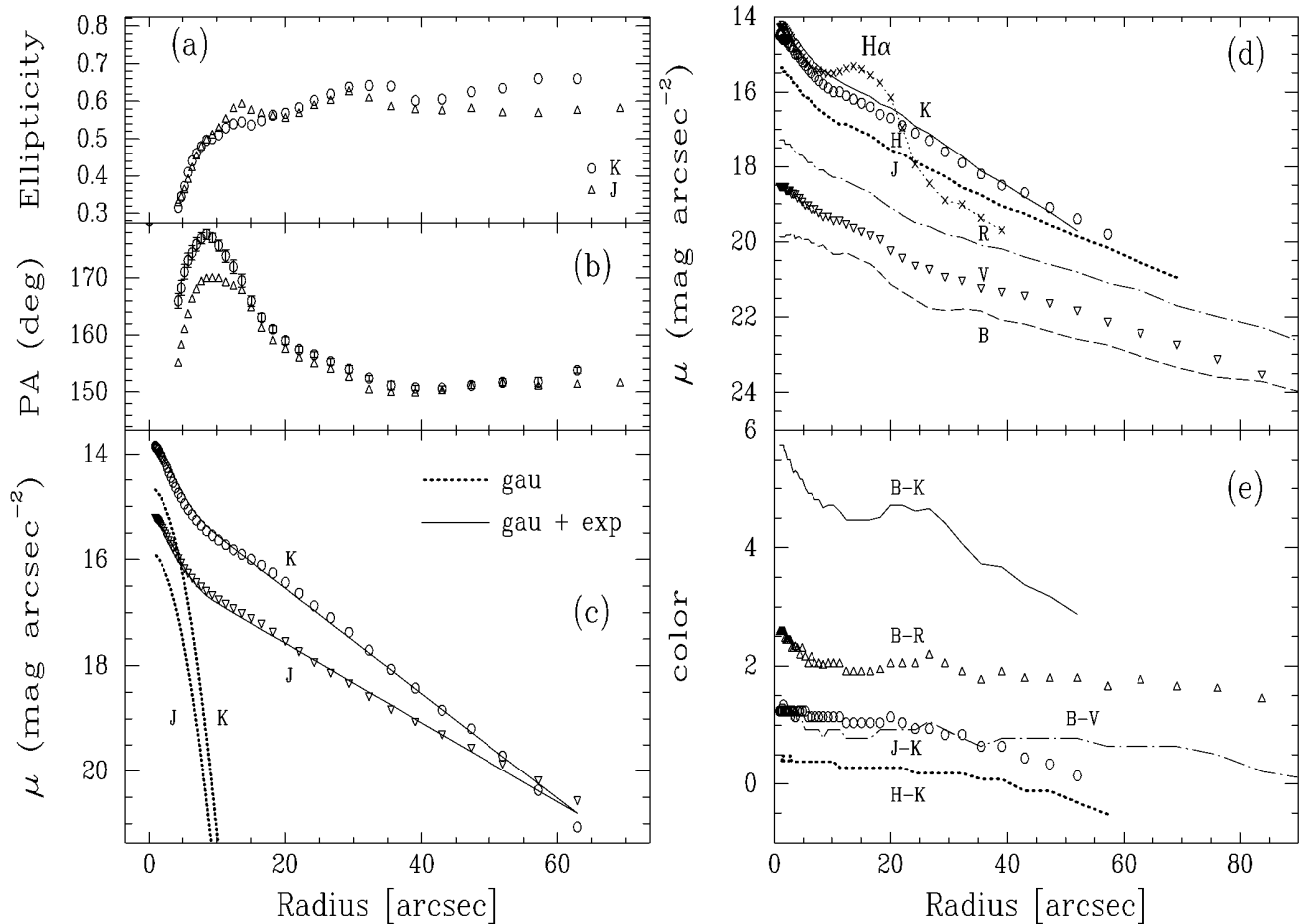


FIG. 3.—Surface photometric analysis of NGC 972. (a) Ellipticity, (b) the major axis P.A., and (c) the surface brightness of the isophotes for *J* and *K* bands are plotted. The observed profiles can be well fitted by a combination of Gaussian (nucleus) and exponential (disk) profiles. The surface brightness profiles in *BVRJHK* bands and the corresponding color profiles are plotted in (d) and (e). For comparison, $H\alpha$ surface brightness profile (expressed in magnitude units with an arbitrary zero point) is also plotted. Note the systematic flattening of the surface brightness profiles from *K* to *B* band—a definite signature of optically thick disks.

central bulge for both *J* and *K* profiles. In Figure 3c, we show the observed intensity profiles in *J* and *K* bands along with the best-fit combination of Gaussian and exponential profiles. The central component corresponds to the nucleus with a Gaussian intensity profile of $\sigma = 4''.0$ (420 pc). The fitted exponential disk has scale lengths of 1.2 and 1.5 kpc in the *K* and *J* bands, respectively.

Thus we conclude that there is no bulge in NGC 972. The central bright spot corresponds to the nucleus. The bar is weak and ends inside a radius of 1 kpc. The disk intensity follows an exponential profile, with a scale length of 1.2 kpc in the *K* band.

3.3. Surface Brightness and Color Profiles

Azimuthally averaged radial intensity profiles in *BVRJHK* bands and in the emission line of $H\alpha$ were obtained by fixing the eccentricity and P.A. corresponding to their values at the outer radii. Prior to profile extraction, the point-spread functions of all of the images are matched (using the IRAF task PSFMATCH) to the one having the poorest seeing ($2''.7$). The resulting intensity and color profiles are shown in Figures 3d and 3e, respectively. It can be easily noticed that the intensity profile in broad bands is the steepest in the *K* band and the flattest in the *B* band. The profiles flatten systematically with decreasing wavelength of the bands. This results in a color gradient with the disk

becoming gradually bluer at outer radii. The nuclear *B–K* color reaches as red as 5.5. The *B–K* color profile shows a red bump between $20''$ and $30''$, which corresponds to the position of the dusty arm.

The $H\alpha$ emission line surface brightness, which is a measure of current star formation, is expressed in magnitude units (with an arbitrary zero point), and hence its profile shape can be directly compared with those in the broad bands. It distinctly differs from other profiles between $10''$ and $25''$, where the profile falls slower than the brightness profiles of old disk stars. This is due to the presence of the brightest $H\ II$ region in the galaxy in this zone. Outside this zone, $H\alpha$ surface brightness falls smoothly.

4. SCALE LENGTHS AND CENTRAL OPTICAL DEPTH

The question about the opacity of galactic disks has drawn a lot of attention in recent years (Burstein, Haynes, & Faber 1991). The availability of data extending from *B* to *K* bands allows us to study the opacity of the disk in NGC 972. One of the quantities that is extensively used for this purpose is the scale length of the exponential disks in different bands (Bothun & Rogers 1992; Evans 1994; Peletier et al. 1994). The underlying stellar disks of galaxies do not show a strong color gradient, and hence the intrinsic (dust-free) scale length of a galactic disk is only weakly dependent on wavelength. However, absorption by dust has the effect

TABLE 1
SCALE LENGTHS OF NGC 972¹

Band	$r_d(\lambda)$ (arcsec)	$r_d(B)/r_d(\lambda)$
<i>K</i>	10.23	2.76
<i>H</i>	13.46	2.10
<i>J</i>	16.41	1.72
<i>R</i>	23.42	1.20
<i>V</i>	24.39	1.16
<i>B</i>	28.21	1.00

¹ Disk profiles between 25" and 65" are used in obtaining the scale lengths.

of flattening the observed intensity profiles, the effect being maximum at shorter wavelengths. Thus, for dusty disks, the scale length observed at the *B* band is expected to be larger than that at the *K* band.

Evans (1994) modeled the wavelength dependence of scale lengths of galaxies for dusty disks. He found that the amount of increase in the scale length at shorter wavelengths depends on the amount of dust (or optical depth) as well as on the relative scale height of dust with respect to that of stars in disks of galaxies. While comparing the observed scale lengths available in the literature to his model results, he noted the necessity of using the same radial zones of intensity profiles to obtain the scale lengths at different wavelengths. Following his suggestions, we obtained scale lengths in *BVRJHK* bands by fitting exponential profiles between an inner radius of 25" and an outer radius of 65" for all of the profiles. The resulting scale length in the *B* band is $r_d(B) = 28.2 = 0.3R_{25} = 3$ kpc. Ratios of *B*-band scale length to that in other bands are given in Table 1. Evans (1994) computed scale lengths at *B*, *I*, and *H* bands for galaxies with and without bulges. Among the computed pure disk models, a model with a dust scale height equal to that of stars can produce the observed scale length ratio $r_d(B)/r_d(H) = 2.1$ for a central optical depth of $\tau_B(0) = 11$. Models including a bulge imply an even higher $\tau_B(0)$ value. Moriondo, Giovanardi, & Hunt (1998) obtained a mean value for the central optical depth in the *V* band of $\tau_V(0) = 2-4$ for a sample of early-type spiral galaxies. Hence, the inferred value of optical depth in NGC 972 is higher than that for normal galaxies, which is not surprising given its dusty appearance. Such high values are also inferred in other dusty galaxies; for example, Evans (1994) estimated a value of $\tau_B(0) = 20$ in the dusty starburst galaxy NGC 253.

5. DISCUSSION

5.1. The Nuclear $H\alpha$ Ring

RP98 reported the presence of a nearly circular star-forming ring of radius 630 pc around the nucleus of NGC 972. Given that the inclination of the galactic disk to the line of sight is 60°, the nuclear ring is either in the galactic plane and intrinsically elliptical, or it is off-planar and intrinsically circular. Classical nuclear rings are circular, lie in the plane of the parent galaxy, and are commonly found in early-type barred galaxies. Such rings are associated with the inner Lindblad resonance (ILR) of galaxies. The existence of ILR in a galaxy depends on the form of the rotation curve in the central parts of galaxies and the pattern speed of the bar or the spiral arm. Burbidge et al. (1965) obtained the rotation curve for the galaxy from slit spectroscopy at

different position angles. They found that the rotation curve in the galaxy rises very slowly, reaching values of around 100 km s⁻¹ at a radius of 25". The galaxy rotates like a solid body at least up to 10" (1 kpc). ILR can exist only outside the solid body rotating region, and hence the observed ring at 630 pc is not a resonance ring.

The H II regions forming the ring can be traced in the optical broad bands, especially in the *B* band, and cannot be traced in any of the NIR bands. In general, nuclear rings in galaxies have stronger continuum compared to the disk H II regions (Kennicutt, Keel, & Blaha 1989). This is understood in terms of a longer history of star formation in circumnuclear H II regions (Korchagin et al. 1995). The absence of a strong continuum in the nuclear ring of NGC 972 indicates that the star formation in the ring has started relatively recently. The formation of the ring is possibly associated with the perturbation caused by a small intruding galaxy (see § 5.3).

5.2. Revision of the Morphological Type of NGC 972

The absence of a bulge even on the NIR images calls for a rediscussion of the adopted Sb morphological classification of NGC 972. In recent years, there have been reports of the absence of classical bulges in galaxies classified as early-type spiral galaxies (Carollo et al. 1997). These may either represent pure misclassifications, considering the subjective nature of the classification, or intrinsic limitations of the criteria used in classification. For example, one of the intrinsic limitations was recently demonstrated by Combes & Elmegreen (1993). Using numerical simulation, they found that bar morphology is more tightly related to the dynamical properties than to the spiral morphology of the galaxy. Thus, a bar with early-type properties can be present in a late-type spiral, as was found recently in NGC 6221 by Vega-Beltrán et al. (1998). Historically used classification criteria do not allow for such mixed characteristics in galaxies.

We compiled all of the existing global properties on NGC 972 in an attempt to clarify its morphological type. In particular, we aim to establish whether it is a misclassified galaxy or has mixed morphological characteristics. The compiled data are presented in Table 2. The parameters in the upper half of the table are related to the morphological type, whereas those in the lower part are related to the starburst properties. The dependence of the listed parameters with morphological type is well established statistically (e.g., Roberts & Haynes 1994). The most likely morphological type for NGC 972, based on each of the observed quantities, is indicated in the third column. Principal morphological indicators, namely the bulge-to-disk ratio and the pitch angle (of the northwest arm measured on the deprojected *K*-band image), are clearly inconsistent with the Sb classification. The dynamical mass, as inferred from the rotational speed, is also too small for the Sb classification. The size of the weak bar is almost equal to the exponential scale length—a condition found to be typical in late-type galaxies (Combes & Elmegreen 1993). Secondary indicators of morphological type such as the neutral hydrogen content and the $H\alpha$ equivalent width (a measure of present to past star formation rate—see Kennicutt & Kent 1983) also suggest a morphological type later than Sc for the galaxy. Observed colors are redder than those found in galaxies of Hubble types Sc and later. However, the prominent stellar population, as indicated by the Yerkes type, is

TABLE 2
MORPHOLOGICAL AND STARBURST PROPERTIES OF NGC 972

Property	Value	Comment	Reference
Morphological Type			
Bulge/disk ratio.....	No bulge	Sd or later	This work
Pitch angle (deg).....	50–60	Sd or later	This work
$V_{\text{rot}}^{\text{max}}$ (km s ⁻¹).....	120	Sc or later	Burbidge et al. 1965
Mass (10 ¹⁰ M _⊙).....	1.2	Sc or later	Burbidge et al. 1965
$M(\text{H I})/M(T)$	0.21	Sd or later	Young et al. 1996
EW (H α) (Å).....	36.4	Sc or later	RP98
$B - V$	0.64	Sb or later	RC3
$U - B$	0.07	Sb or later	RC3
Yerkes Type.....	F3	~Sc	Humason, Mayal, & Sandage 1956
Mean Type.....	...	Sd	...
Starburst Properties			
$L(\text{FIR})$ (10 ¹⁰ L _⊙).....	3.67	1.15 × M82	Young et al. 1996
$L_{\text{H}\alpha}$ (10 ⁴¹ ergs s ⁻¹).....	2.95	0.85 × M82	RP98; Young et al. 1996
Star formation rate (M _⊙ yr ⁻¹).....	2.64	0.85 × M82	RP98
$M(\text{H}_2)/M(\text{H I})$	1.41	1.70 × M82	Young et al. 1996
$M(\text{H I} + \text{H}_2)/M(T)$	0.50	...	Young et al. 1996

not consistent with the red colors, suggesting that the galaxy may have intrinsically blue color typical of late-type spirals but is reddened by the heavy amount of dust in the galaxy. Thus, all of the global properties suggest a morphological type later than Sc. The galaxy, however, has several peculiarities, the most striking one being the absence of a stellar arm accompanying the dusty arm on the southeast side. Thus the most appropriate morphological type for NGC 972 would be SABd pec.

5.3. Is NGC 972 the Result of a Minor Merger?

The far-infrared and H α luminosities suggest a high rate of recent star formation in NGC 972. Nuclear starburst, whose properties compare well with that of other well-known starbursts, contributes to most of this star formation (Table 2; see also RP98). Starburst activity is common in galaxies having an interacting companion or in galaxies formed due to merging of two nearly equal-mass systems. The chaotic distribution of dust lanes in NGC 972 gives it a close resemblance in appearance to the starburst galaxy M82. The present activity of M82 is known to be triggered due to its interaction with M81 (Ichikawa et al. 1994; Yun, Ho, & Lo 1994). However, there is no galaxy visible on the Palomar Sky Survey prints within 10 times the optical diameter with a velocity difference less than 1000 km s⁻¹ of NGC 972 (Solomon & Sage 1988). The galaxy does not show any obvious signatures of a merger such as tidal tails or bridges. Thus it is safe to assume that NGC 972 is an isolated galaxy. Among the isolated galaxies, starbursts are most commonly associated with a strong bar. Absence of a strong bar in NGC 972 calls for invoking alternative mechanisms for triggering the activity in this galaxy. One such alternative mechanism is a merger with a low-mass companion object, such as a dwarf galaxy (minor merger).

NGC 972 at present contains an unusually high amount of its mass (50%) in the gaseous form, with the molecular mass exceeding the atomic mass (Young et al. 1996). Such a high ratio of molecular to atomic mass is typical of that found in optically distorted and merging galaxies (Mirabel & Sanders 1989), which gives independent support for possibly merger-induced starburst activity in this galaxy. The NGC 972 group of galaxies contains many dwarf spher-

oidals (Vennick & Richter 1994), and hence a merger with one of those galaxies in the recent past cannot be ruled out. If that is the case, the merged dwarf spheroidal galaxy had to be gas rich. However, dwarf spheroidal galaxies are normally poor in gas content. On the other hand, small gas clouds (mass less than 10% of the primary galaxy) are known to exist around several galaxies (Schulman, Bregman, & Roberts 1994), the most familiar example being the high-velocity clouds around our own Milky Way. Accretion of such clouds can naturally enhance the gas mass in the galaxy. As the accreted gas flows to the center of the galaxy, it transforms to molecular form, triggering the intense burst seen in the galaxy. The accretion process is probably responsible for the off-planar nuclear ring. In such a scenario, the plane of the ring may represent the plane in which the gas is being accreted.

NGC 972 is very asymmetric, with its northwest arm much stronger than the southeast arm in the stellar continuum. Such an asymmetry is common in late-type galaxies containing a companion (Odewahn 1994). In a recent study, Pisano, Wilcots, & Elmegreen (1998) argue that the observed morphological and kinematical asymmetries in the late-type galaxy NGC 925 are due to one or many interactions with a companion low-mass galaxy. They discovered an H I cloud of mass 10⁷ M_⊙ in the neighborhood of the galaxy, which they believe is the residual gas cloud resulting from the interactions. Thus it is very likely that the observed asymmetry in NGC 972 is caused by the minor merger of a gas-rich companion, which, as we discussed above, can also account for the observed starburst activity, high molecular gas fraction, and the off-planar nuclear ring. It however remains to be seen whether gas clouds, such as that found in NGC 925, also surround NGC 972. This is one of the issues that we will be investigating in the future.

6. CONCLUSIONS

We carried out a detailed analysis of the morphological type of NGC 972 using a variety of physical parameters. We favor a morphological type as late as Sd based on the absence of a bulge, the high pitch angle of the spiral arm, the low dynamical mass, and the high mass fraction in gas. However, it was classified as Sb and I0 in major astronomi-

cal catalogs and atlases, which were mainly guided by the morphological appearance of dust lanes rather than a detailed quantitative analysis such as that carried out here. The galaxy contains a heavy amount of dust with central B -band face-on optical depth as high as $\tau_B(0) = 11$. The spiral arms are asymmetric, with the northwest spiral arm brighter than the southeast spiral in the stellar continuum. The galactic nucleus is undergoing a starburst with a strength comparable to that in M82. In addition, there is active star formation in an off-planar nuclear ring, and the galaxy is extremely gas rich, especially in molecular form. We propose that all of these activities are a result of a merger of NGC 972 with a gas-rich companion.

We thank the time allocation committee of the Observatorio Astronómico Nacional for granting us the telescope time for NIR observations. We also thank Olga Kuhn for her excellent support as resident astronomer at the observatory and Ivanio Puerari for reading the manuscript. The Digitized Sky Surveys were produced at the Space Telescope Science Institute under US government grant NAGW-2166. The images of these surveys are based on photographic data obtained using the Oschin Schmidt Telescope on Palomar Mountain and the UK Schmidt Telescope. This work has been partially supported by CONACYT research grants 211290-5-25869E and 211290-5-1430PE.

REFERENCES

- Bothun, G. D., & Rogers, C. 1992, *AJ*, 103, 1484
 Burbidge, E. M., Burbidge, G. R., & Prendergast, K. H. 1965, *ApJ*, 142, 649
 Burstein, D., Haynes, M. P., & Faber, S. M. 1991, *Nature*, 353, 515
 Carollo, C. M., Stiavelli, M., de Zeeuw, P. T., & Mack, J. 1997, *AJ*, 114, 2366
 Casali, M. M., & Hawarden, T. 1992, *The JCMT-UKIRT Facility Newsl.*, 4, 33
 Combes, F., & Elmegreen, B. G. 1993, *A&A*, 271, 391
 Cruz-Gonzalez, I., et al. 1994, *Rev. Mexicana Astron. Astrofis.*, 29, 197
 de Jong, R. S. 1996, *A&A*, 313, 377
 de Vaucouleurs, G., de Vaucouleurs, A., & Corwin, H. G. 1976, *Second Reference Catalogue of Bright Galaxies* (Austin: Univ. Texas Press)
 de Vaucouleurs, G., et al. 1991, *Third Reference Catalogue of Bright Galaxies* (New York: Springer) (RC3)
 Evans, R. 1994, *MNRAS*, 266, 511
 Humason, M., Mayal, N. U., & Sandage, A. 1956, *AJ*, 60, 254
 Ichikawa, T., van Driel, W., Aoki, T., Soyano, T., Tarusawa, K., & Yoshida, S. 1994, *ApJ*, 433, 645
 Kennicutt, R. C., Keel, W. C., & Blaha, C. A. 1989, *AJ*, 97, 1022
 Kennicutt, R. C., & Kent, S. M. 1983, *AJ*, 88, 1094
 Knapen, J. H., Beckman, J. E., Heller, C. H., Shlosman, I., & de Jong, R. S. 1995, *ApJ*, 454, 623
 Korchagin, V., Kembhavi, A. K., Mayya, Y. D., & Prabhu, T. P. 1995, *ApJ*, 446, 574
 Krienke, O. K., & Hodge, P. W. 1974, *AJ*, 79, 1242
 Mirabel, I. F., & Sanders, D. B. 1989, *ApJ*, 340, L53
 Moriondo, G., Giovanardi, C., & Hunt, L. K. 1998, *A&AS*, 130, 81
 Odewahn, S. 1994, *AJ*, 107, 1320
 Peletier, R. F., Valentijn, E. A., Moorwood, A. F. M., & Freudling, W. F. 1994, *A&AS*, 108, 621
 Pisano, D. J., Wilcots, W. M., & Elmegreen, B. G. 1998, *AJ*, 115, 975
 Ravindranath, S., & Prabhu, T. P. 1998, *AJ*, 115, 2320 (RP98)
 Roberts, M. S., & Haynes, M. P. 1994, *ARA&A*, 32, 115
 Sandage, A. R. 1961, *Hubble Atlas of Galaxies* (Washington: Carnegie Institution of Washington)
 Sandage, A. R., & Tammann, G. A. 1981, *A Revised Shapely-Ames Catalogue of Bright Galaxies* (Pub. 635; Washington: Carnegie Institution of Washington)
 Schulman, E., Bregman, J. B., & Roberts, M. S. 1994, *ApJ*, 423, 180
 Solomon, P. M., & Sage, L. J. 1988, *ApJ*, 334, 613
 Vega-Beltrán, J. C., et al. 1998, *A&AS*, 131, 105
 Vennick, J., & Richter, G. M. 1994, *Astron. Nachr.*, 315, 245
 Young, J. S., Allen, L., Kenny, J. D., Lesser, A., & Rownd, B. 1996, *AJ*, 112, 1903
 Yun, M. S., Ho, P. T. P., & Lo, K. Y. 1994, *Nature*, 372, 530
 Zaritsky, D. 1993, *PASP*, 105, 1006
 Zaritsky, D., Rix, H.-W., & Rieke, M. 1993, *Nature*, 364, 313